J Comput Aided Mol Des (2006) 20:495–509
DOI 10.1007/s10822-006-9068-9

ORIGINAL PAPER

Cannabinoid CB1 receptor recognition of endocannabinoids via the lipid bilayer: molecular dynamics simulations of CB1 transmembrane helix 6 and anandamide in a phospholipid bilayer

Diane L. Lynch · Patricia H. Reggio

Received: 28 June 2006 / Accepted: 15 August 2006 / Published online: 14 November 2006

Abstract The phospholipid bilayer plays a central role in the lifecycle of the endogenous cannabinoid, *N*-arachidonoylethanolamine (anandamide, AEA). Therefore, the orientation and location of AEA in the phospholipid bilayer with respect to key membrane associated proteins, is a central issue in understanding the mechanism of endocannabinoid signaling. In this paper, we report a test of the hypothesis that a $\beta XX\beta$ motif (formed by beta branching amino acids, V6.43 and I6.46) on the lipid face of the cannabinoid CB1 receptor in its inactive state may serve as an initial CB1 interaction site for AEA. Eight 6 ns NAMD2 molecular dynamics simulations of AEA were conducted in a model system composed of CB1 transmembrane helix 6 (TMH6) in a 1,2-dioleoyl-*sn*-glycero-3-phosphocholine (DOPC) bilayer. In addition, eight 6 ns NAMD2 molecular dynamics simulations of a low CB1 affinity (20:2, *n*–6) analog of AEA were conducted in the same model system. AEA was found to exhibit a higher incidence of V6.43/I6.46 groove insertion than did the (20:2, *n*–6) analog. In certain cases, AEA established a high energy of interaction with TMH6 by first associating with the V6.43/I6.46 groove and then molding itself to the lipid face of TMH6 to establish a hydrogen bonding interaction with the exposed backbone carbonyl of P6.50. Based upon these results, we propose that the formation of this hydrogen bonded AEA/TMH6 complex may be the initial step in CB1 recognition of AEA in the lipid bilayer.

Keywords Anandamide · Bilayer · Cannabinoid · CB1 · Endocannabinoid · GPCR · Lipid · Molecular dynamics · Groove

Abbreviations

AEA	*N*-arachidonoylethanolamine
CB1	Cannabinoid Receptor Type 1
CM	Conformational Memories
FAAH	fatty acid amide hydrolase
GPCR	G protein-coupled receptor
Rho	Rhodopsin

Introduction

The phospholipid bilayer plays a central role in the lifecycle of the endogenous cannabinoid, *N*-arachidonoylethanolamine (anandamide, AEA, **1**). AEA has been shown to be synthesized from lipid [1, 2], to interact with the membrane embedded cannabinoid CB1 receptor [3], to be transported to intracellular compartments possibly via caveolae related endocytosis [4] and finally to be degraded by fatty acid amide hydrolase (FAAH), an integral membrane protein whose active site is accessed by AEA possibly via the bilayer [5]. Therefore, the location of AEA in the phospholipid bilayer, as well as its orientation with respect to key membrane associated proteins, is a central issue in understanding the mechanism of endocannabinoid signaling.

D. L. Lynch · P. H. Reggio (✉)
Center for Drug Design, Department of Chemistry and Biochemistry, University of North Carolina Greensboro, 435 New Science Building, P.O. Box 26170, Greensboro, NC 27402-6170, USA
e-mail: phreggio@uncg.edu

The cannabinoid CB1 receptor is a Class A G protein-coupled receptor (GPCR) [6]. Several other endogenous cannabinoids have been identified in addition to AEA that bind to CB1, including sn-2-arachidonoylglycerol (2-AG, **2**) [7], 2-arachidonyl glyceryl ether (**3**) [8] and *O*-arachidonoylethanolamine (virodhamine, **4**) [9]. These endocannabinoids possess a variety of head groups (see Chart 1), but all are derivatives of arachidonic acid. As can be seen in Chart 1, arachidonic acid (**5**) is a 20 carbon fatty acid with four cis double bonds separated by methylene carbons (i.e., four homoallylic double bonds). The first double bond in **5** starts at the sixth carbon atom from the tail of the fatty acid. It is therefore described as a (20:4, *n*–6) fatty acid. Consistent with the variation seen in head groups between **1–4** is the fact that endocannabinoid SAR indicates the CB1 receptor does not tolerate large endocannabinoid head groups, however, it does recognize a wide variety of both polar and non-polar moieties in the head group region [10–12]. Consistent with the fact that all four natural endogenous cannabinoids (**1–4**) are arachidonic acid derivatives is a very restrictive acyl chain SAR which indicates CB1 binds only *n*–6 fatty acids with 20–22 carbons and at least three homoallylic double bonds. This SAR is illustrated by the following series of ethanolamides and their CB1 affinities: 22:4, *n*–6 (K_i = 34.4 ± 3.2 nM), 20:4, *n*–6 (K_i = 39.2 ± 5.7 nM; **1**), 20:3, *n*–6 (K_i = 53.4 ± 5.5 nM); and, 20:2, *n*–6 (K_i = 1500 nM; **6**) [13]. Double bond conjugation within the acyl chain results in diminished CB1 affinity [14, 15] and numerous attempts to rigidify the acyl chain into a particular conformation by ring formation have resulted in compounds lacking CB1 affinity [16–18].

The endocannabinoid requirement for *n*–6 fatty acids (i.e., a saturated pentyl tail) parallels the

Chart 1

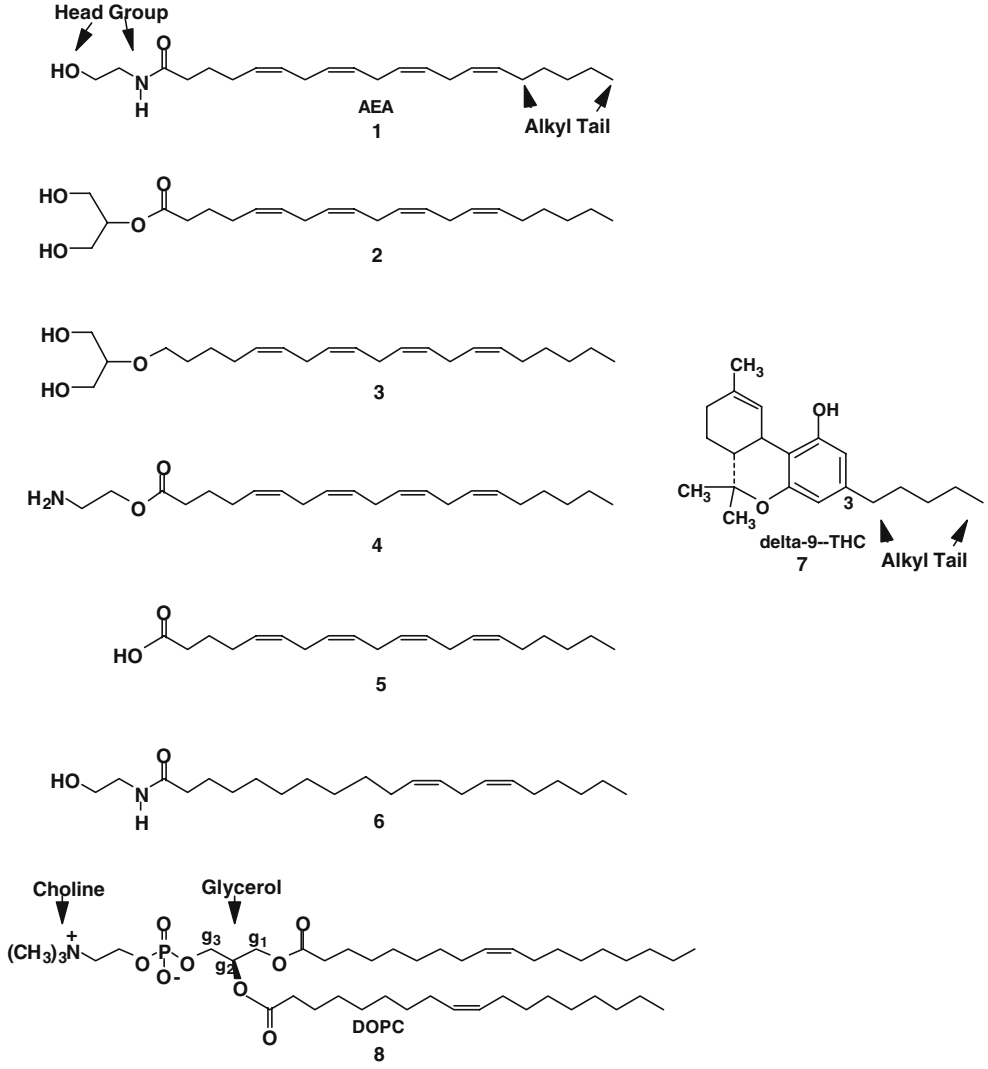

requirement for an alkyl chain with no less than five carbons for highly lipophilic classical cannabinoid compounds such as Δ^9-THC (**7**) [10]. In fact, cannabinoid SAR studies have shown that no matter the number of hydrogen bonding moieties attached to a classical cannabinoid fused ring structure, a C-3 alkyl tail shorter than five carbons results in *complete loss* of CB1 affinity. These alkyl/acyl chain parallels between the classical/endogenous cannabinoids, combined with the high lipophilicities of both classes of compounds, led us to hypothesise that the lipid environment may orient classical/endogenous cannabinoids for initial receptor interaction. Further, we have hypothesized that these alkyl/acyl chain length requirements may actually be membrane depth requirements for ligands to reach a recognition site on the lipid face of CB1 that can initially ''fish'' these ligands out of lipid.

Ballesteros has proposed that β-branching residues (Val, Ile, or Thr) located (i,i + 3) or (i,i + 4) apart on an α-helix can form a hydrophobic groove into which an alkyl chain can fit [19]. Transmembrane helix 6 (TMH 6) in the CB receptors is rich in beta branched amino acids (V, I, or T). In the CB1 inactive state, two runs of β-branched amino acids create grooves on Helix 6: (1) residues V6.38, V6.42, and I6.45 form a groove that is located in the TMH 5–6 interface; while, (2) V6.43 and I6.46 form a groove on the *lipid face* of TMH 6 close to the TMH 6–7 interface. We have hypothesized that this V6.43/I6.46 groove located immediately intracellular to the CWXP motif in the CB receptors is the initial interaction site for classical/endogenous cannabinoids. Recent CB1 V6.43A/I6.46A double mutation studies have shown that this mutation leads to a complete separation of the binding pockets of classical/endogenous cannabinoids from all other cannabinoid structural classes [20]. Two newly deorphanized cannabinoid receptors, GPR55 [21, 22] and GPR35 [23] also have a groove formed by β-branchers at these same positions (V6.43/V6.46).

In this paper, we report a test of the hypothesis that the CB1 V6.43/I6.46 groove may serve as an initial CB1 interaction site for the endogenous cannabinoid anandamide (AEA, **1**). To this end, we conducted 48 ns molecular dynamics (MD) simulations of either AEA or its low CB1 affinity (20:2, *n*–6) analog (analog, **6**, K_i = 1500 nM) in a model system composed of CB1 TMH6 in a 1,2-dioleoyl-*sn*-glycero-3-phosphocholine (DOPC; **8**) bilayer. We show that AEA exhibits a higher incidence of V6.43/I6.46 groove insertion than does the (20:2, *n*–6) analog. In certain cases, AEA (but not the Analog) can establish a high energy of interaction with TMH6 by first associating with the V6.43/I6.46 groove and then molding itself to the lipid face of TMH6 to establish a hydrogen bonding interaction with the exposed backbone carbonyl of P6.50.

Methods

Eight simulations (6 ns each) of AEA/TMH6/DOPC and eight simulations (6 ns each) of Analog/TMH6/DOPC were undertaken here. We divided the simulations into 6 ns segments in order to explore the effect of different anandamide/analog starting positions. The segment length was also chosen to avoid possible deformation from helicity that might occur in TMH6 over long simulation times since TMH6 in these simulations does not benefit from being part of a TMH bundle.

The sixteen 6 ns simulations employed the NAMD2 [24] molecular dynamics software package with the CHARMM27 parameter set [25–27] including data for polyunsaturated lipids [28], along with the TIP3P model for water. Force field parameters for AEA (**1**) and for its (20:2, *n*–6) analog (**6**) were constructed by utilizing existing parameters for similar atom types. For example, the polyunsaturated acyl chain parameters necessary for the hydrocarbon chain of **1** and **6** are included in the current lipid force field [28]. Amide and hydroxyl values were taken from the serine amino acid parameter set. Periodic boundary conditions were employed with the long range coulombic electrostatic potential treated with the Particle Mesh Ewald summation method [29] and the Lennard–Jones potential was smoothly cut-off between 8.5 Å and 10 Å. The NAMD2 simulations reported here used the r-RESPA multiple time step algorithm with a time step of 4 fs for long-range electrostatic forces, 2 fs for short-range nonbonded forces, and 1 fs otherwise. In production runs, configurations were stored every 1 ps for later analysis.

The initial configuration for TMH 6 and AEA(**1**) (or TMH6 and Analog (**6**)) in 1,2-dioleoyl-*sn*-glycero-3-phosphocholine (DOPC, **8**) (see chemical structures for **1**, **6** and **8** in Chart 1) was constructed as follows: First a high hydration bilayer patch of DOPC (72 lipid molecules with 36 in each leaflet) was generated as described in our recent paper [30]. Using a snapshot from the pure DOPC simulation, two DOPC molecules were removed from each leaflet, and CB1 TMH6 (Sequence: RMDIRLAKTLVLILVVLIICWGPLLAIMVYDVFGK; proline kink angle = 53.1°; charges neutralized) was inserted in their place. Then an additional DOPC molecule adjacent to TMH6 from the outer leaflet was removed and **1** or **6** was inserted. This kept the total number of atoms nearly constant. The simulation cell contained a total of 16084 atoms

(AEA) or 16088 atoms (Analog). Compound **1** or **6** was inserted close to TMH6 so that simulation time was not lost to diffusion.

Steric overlap between the initially placed TMH6, **1** (or **6**) and lipid/water molecules was relieved by allowing the latter to adiabatically relax in the presence TMH6 and **1** or **6**. This was achieved by freezing the positions of the atoms in TMH6 and **1** or **6** and performing an energy minimization of 5,000 steps. The backbone of TMH6 and the heavy atoms of **1** or **6** were then constrained with a harmonic force (k = 0.5 kcal/mol Å^2) and an energy minimization of 5000 steps was performed. If the groove was occupied by a lipid acyl chain after this minimization, the lipid acyl chain was moved and the acyl tail of **1** or **6** was inserted in the groove, followed by a 5,000 step minimization. We did not place ligands on other faces of TMH6, because in the context of the entire CB1 TMH bundle, only the face including V6.43/I6.46 faces lipid in the CB1 inactive state.

Subsequently, the system was heated in 50 K steps from 0 K to 310 K (physiological conditions) at constant volume (NVT ensemble), using Langevin coupling to a heat bath [31], equilibrating for 0.1 ns per interval with the heavy atoms in TMH6 and **1** or **6** constrained by a harmonic force (k = 0.5 kcal/mol Å^2). Using the NVT ensemble at 310 K, the heavy atom constraints on TMH6 and **1/6** were released in five steps (k = 0.4, 0.3, 0.2, 0.1, 0.05 kcal/mol/Å^2) of 0.1 ns each. At this point unconstrained heating in the NVT ensemble lead to χ1 torsion angle flipping on C6.47/I6.46/V6.43, so these dihedrals were restrained by a harmonic force (k = 3 kcal/mol Å^2 for **1** and k = 10 kcal/mol Å^2 for **6**) for 0.1 ns at 310 K (NVT ensemble). Because there were fewer contacts made between the acyl tail of the analog (**6**) and the V6.43/I6.46 groove, we saw more χ1 torsion angle fluctuations that could preclude acyl tail/groove interaction. In order to maximize the chance that the acyl tail would find the groove, we used higher restraints on the χ1 s in the simulations of TMH6 and **6**.

The ensemble was switched to NPT (310 K/1 atm) and run for 1 ns with strong coupling to the pressure bath. From this starting point, the coordinates and velocities were used in eight very short MD runs of 50 ps each for **1** and for **6** to scramble the velocities and positions somewhat. This resulted in non-identical positions for the ligand relative to TMH6 that could be used as starting points for production runs. Each of these was then run (NPT, 310 K/1 atm) for 6 ns (the first 4 ns were run with the constraints on the dihedrals discussed above and then 2 ns unconstrained), resulting in eight 6 ns trajectories for TMH6/**1** and eight 6 ns trajectories for TMH6/**6**.

Re-run of AEA Run 4

In order to ascertain if interactions seen in AEA Run 4 could be reproduced, a snapshot from Run 4 (t = 2720 ns) was energy minimized. The system was then heated to 310 K in 10° increments, while the atoms of TMH6 and **1** were restrained (harmonic force, k = 0.5 kcal/mol/Å^2). These restraints were gradually released using a force constant of 0.5 kcal/mol/Å^2 to 0.05 kcal/mol/Å^2 over 0.6 ns and a 6 ns run was initiated using the NPT ensemble (310 K/1 atm).

Trajectory analysis

All MD trajectories were analyzed in order to determine the structural and dynamical properties of each system in DOPC. Analysis of these trajectories characterized: (i) whether or not the acyl tail of **1/6** was inserted into the V6.43/I6.46 groove; (ii) the frequency with which lipid interacted with the V6.43/I6.46 groove; (iii) the stability of the helix over the trajectory; (iv) the energy of interaction of **1/6** with TMH6; (v) the inter- and intramolecular hydrogen bonding patterns of the polar headgroup of **1/6**; and, (vi) the location in the lipid bilayer of the polar headgroup of **1/6**, as well as the terminal methyl group of **1/6**.

Hydrogen bonding analysis

The Hbond analysis facility of VMD [32] was used to analyze the trajectories for the incidence of hydrogen bonding. Interactions for which the heteroatom to heteroatom distance was 3.5 Å or less, with X–H–X angles between 180° to 120° were considered hydrogen bonds.

Energy and helix stability analyses

The energy analysis reported here is similar to that reported by Elmore and Dougherty [33]. Specifically, interaction energies between ligand and TMH6 were calculated using the pair interaction energy capability of NAMD2 [24] with a 25 Å cutoff for interaction energies. To analyze the stability of TMH6 throughout the trajectory, the RMSD of the helix backbone relative to the starting structure was monitored for each production run.

Acyl Tail/Lipid acyl chain insertion into groove

Receptor residues are numbered here using the amino acid numbering scheme proposed by Ballesteros and Weinstein [34]. In this numbering system, the most

highly conserved residue in each TMH is assigned a locant of 0.50. This number is preceded by the TMH number and can be followed in parentheses by the sequence number. All other residues in a TMH are numbered relative to this residue. In this numbering system, for example, the most highly conserved TMH6 residue of the CB1 receptor is P6.50(358). The residue that immediately precedes it is G6.49(357).

Each picosecond stored frame of the trajectories was screened for acyl tail insertion into the V6.43/I6.46 groove. The acyl tail was counted as inserted into the groove if it met both of the following criteria: (1) *any* of the carbons in the pentyl tail of **1** or **6** were within 4.5 Å of *any* of the carbon atoms that make up the sidechain of V6.43 and simultaneously *any* of the carbon atoms that make up the sidechain of I6.46; and (2) a vector drawn from C-beta of I6.46 to C-beta of V6.43 makes an angle between 25° and 155° with a vector drawn from the atom in the acyl tail that is in contact with I6.46 to the atom that is in contact with V6.43. The frequency of insertion was broken down for each nanosecond of the trajectory and is illustrated in Table 1 for AEA and the Analog. Analyses of lipid interaction with the V6.43/I6.46 groove focused on the last five carbons of the lipid acyl chain (sn–1 or sn–2) and used the same protocol as described above for ligand acyl chains.

Group distributions

The distributions pictured in Fig. 2 (a and b) were previously obtained [30]. Taking the *z*-direction as normal to the plane of the membrane, the group distributions in Fig. 3 were obtained by slicing along this direction and counting the number of heavy atoms in each functional group in each slice. To obtain a smooth graph, 200 slices were used. This produces a density per unit volume as a function of *z* for each time step in the simulation. The choline distribution was then averaged over the course of the MD simulation, while the AEA distributions were averaged over the time slice indicated in each figure. The distributions were left unscaled.

Results

The purpose of the multisecond MD simulations undertaken here was to determine in a model system composed of DOPC and CB1 TMH6, if AEA (**1**) or its (20:2, *n*–6) analog (**6**) were capable of interacting with the V6.43/I6.46 groove and if there were any differences in the interaction properties of AEA with TMH6 versus its low CB1 affinity Analog subsequent to groove interaction.

Frequency of V6.43/I6.46 groove occupancy

Table 1 presents a summary of the number of picosecond frames in each nanosecond of the trajectory for which the alkyl/acyl tail of AEA (**1**) versus the Analog (**6**) (see Chart 1) interacted with the V6.43/I6.46 groove. It is clear here that the incidence of tail/groove interaction was higher for AEA than for the Analog. AEA had (>50 ps) tail/groove interactions in three or more nanoseconds of the trajectory (Runs 1, 3, 4 and 7). No Analog runs reached this level.

Interaction energies

We have chosen to profile completely here a sub-set of the runs detailed in Table 1. This set includes runs for which groove interaction was highest (AEA Run 4 (6 ns) and Analog Run 2 (first 2 ns)) and a second set of runs for which groove interaction was less frequent (AEA Run 7 (6 ns) and Analog Run 1 (first 2 ns)). RMSD plots for TMH6 (not shown) revealed that

Table 1 Frequency of AEA or Analog alkyl tail/groove interaction (ps/ns time frame) over length of full trajectory

	AEA						Analog					
	1 ns	2 ns	3 ns	4 ns	5 ns	6 ns	1 ns	2 ns	3 ns	4 ns	5 ns	6 ns
Run 1	672	452	748	3	0	3	1	130	2	0	0	0
Run 2	87	0	0	0	31	0	526	252	5	0	0	0
Run 3	168	62	91	1	0	0	0	0	0	0	0	0
Run 4	556	361	599	358	261	3	0	0	0	0	0	0
Run 5	170	2	0	0	101	0	0	0	0	0	0	0
Run 6	41	10	38	17	0	0	122	1	0	8	16	0
Run 7	1	35	21	67	232	267	0	0	2	0	0	0
Run 8	2	106	77	13	35	14	12	0	2	0	0	0
Sum	1697	1028	1574	459	660	287	661	383	11	8	16	0
Average	212.1	128.5	196.8	57.4	82.5	35.9	82.6	47.9	1.38	1.00	2.00	0.00
% Occup	21.21	12.85	19.68	5.74	8.25	3.59	8.26	4.79	0.14	0.10	0.20	0.00

TMH6 was stable through these trajectory segments. Table 2 presents the energy of interaction between each ligand and TMH6 averaged over the part of the trajectory where a groove interaction occurred. For AEA Runs 4 and 7, groove interaction spanned the full 6 ns, whereas for the Analog, groove interaction occurred during the first 2 ns. As is indicated in Table 2, the total interaction energy of AEA Run 4 was statistically different at the $p = 0.05$ level from the total interaction energy for AEA Run 7. For the Analog, the energy of interaction with TMH6 over the period of groove insertion (2 ns) was higher for Run 2 in which groove insertion was higher, but neither of the TMH6/Analog interaction energies were statistically different from the energies for AEA Run 7. Closer analysis of the AEA Run 4 trajectory revealed that the initial groove interaction was followed by the formation of a specific hydrogen bond between the AEA amide –NH and the exposed P6.50 backbone carbonyl oxygen that promoted a tight association of AEA with TMH6. This hydrogen bond is facilitated by a sequence dictated larger than typical proline kink angle in CB1 TMH6 (see Discussion).

The trajectories were also analyzed for the incidence of lipid acyl chain interaction with the V6.43/I6.46 groove. Interaction with the groove occurred predominantly with the sn–1 chain of lipids from the inner leaflet of the bilayer in both the AEA and Analog runs. For the AEA/TMH6 Runs 4 and 7, lipids interacted 9.05% and 8.40% of the time, respectively. For the Analog/TMH6 Runs 1 and 2, lipids interacted 63.25% and 25.15%, respectively.

Hydrogen bonding interactions

In our previous 10 ns MD study of AEA in DOPC, we found that AEA hydrogen bonding was widespread but of short duration, as individual hydrogen bonds lasted ~0.10–0.25 ns [30]. In these simulations, the occurrence of AEA –OH group hydrogen bonds with water (that had penetrated into the bilayer), the DOPC phosphate group and the DOPC ester group was found to be 66.20%, 22.90% and 4.50%, respectively. The occurrence of AEA amide –NH hydrogen bonds with water (that had penetrated into the bilayer), the DOPC phosphate group and the DOPC ester group was found to be 69.00%, 2.70% and 14.20%, respectively. Intramolecular hydrogen bonding between the amide –NH and hydroxyl oxygen had only a 5.10% occurrence.

Table 2 Average TMH6 energy of interaction with AEA or Analog

Run	Ligand/TMH6 average energy		
	Elec (SD) kcal/mol	VDW (SD) kcal/mol	Total (SD) kcal/mol
AEA 4[a]	–2.64(2.02)	–19.43(2.87)	–22.07(4.0)[b]
AEA 7[a]	–0.82(1.69)	–11.65(2.53)	–12.47(3.29)
Anlg 1[c]	–0.25(0.70)	–12.77(1.81)	–13.04(1.88)
Anlg 2[c]	–0.64(0.78)	–14.36(2.20)	–15.00(2.26)

[a] Energy averaged over 6 ns of trajectory

[b] The total interaction energy of AEA Run 4 was statistically different at the $p = 0.05$ level from the total interaction energies for AEA Run 7, Analog Run 1 or Analog Run 2

[c] Energy averaged over first 2 ns of trajectory

AEA results

AEA maintained hydrogen bonding distance with the P6.50 carbonyl oxygen for ~3.5 ns of the Run 4 trajectory (see Fig. 1). A re-run of Run 4 (see Methods) resulted in hydrogen bonding distance maintained over ~5.0 ns of the trajectory (data not shown). Using both heteroatom distance and hydrogen bond angle criteria, this close distance qualified as a hydrogen bond for 33.17% of the trajectory (see Table 3). In Run 4, the AEA amide –NH group also has a hydrogen bond with water (that had penetrated into the bilayer) over 36.00% of the trajectory. The hydroxyl group acts as a hydrogen bond donor to water, the DOPC phosphate and the DOPC ester for 91.17%, 1.33% and 4.50% of

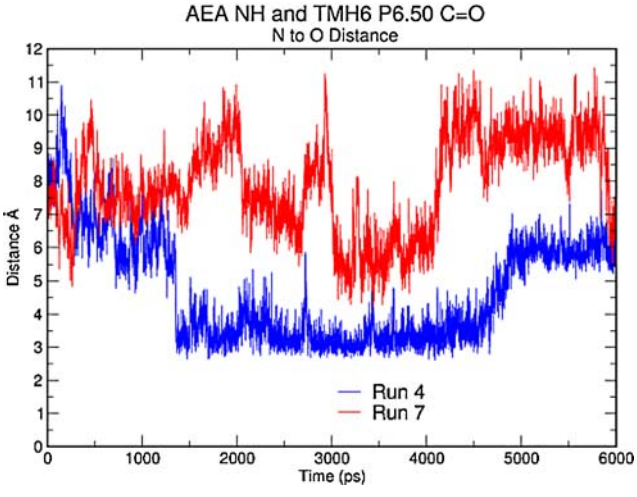

Fig. 1 This graph illustrates the AEA amide –NH to TMH6 P6.50 carbonyl oxygen distance as a function of time over two 6 ns NAMD2 runs for AEA/TMH6 in DOPC. Run 4 results are shown in blue, while Run 7 results are shown in red. In Run 4, the amide –NH and P6.50 carbonyl oxygen maintained hydrogen bonding distance for ~3.5 ns. These groups did not achieve such close distances in Run 7

Table 3 Hydrogen Bonding of AEA or Analog with TMH6 or bilayer constituents in selected runs

TMH6 or Bilayer Constituent	AEA Run 4 Headgroup			AEA Run 7 Headgroup			Analog Run 1 Headgroup			Analog Run 2 Headgroup		
	–NH Average % Time H Bond Formed	–OH Donor Average % Time H Bond Formed	–OH Acceptor Average % Time H Bond Formed	–NH Average % Time H Bond Formed	–OH Donor Average % Time H Bond Formed	–OH Acceptor Average % Time H Bond Formed	–NH Average % Time H Bond Formed	–OH Donor Average % Time H Bond Formed	–OH Acceptor Average % Time H Bond Formed	–NH Average % Time H Bond Formed	–OH Donor Average % Time H Bond Formed	–OH Acceptor Average % Time H Bond Formed
P6.50 C = 0	33.17											
Water[a]	36.00	91.17	79.50	68.83	80.17	80.50		88.50	86.00		7.00	96.50
DOPC (PO_4)		1.33			13.50			8.00			90.50	
DOPC (ester)		4.50		8.67	2.83		83.00	1.00		89.50	1.50	
No H Bond	30.83	3.00	20.50	22.50	3.50	19.50	17.00	2.50	14.00	10.50	1.00	3.50

[a] These are water molecules that have penetrated into the phospholipid headgroup region (see Fig. 2a)

the trajectory, respectively. The hydroxyl group acts as a hydrogen bond acceptor to water over 79.50% of the trajectory.

In Run 7, the AEA amide –NH group never comes close enough to the backbone carbonyl of P6.50 to establish a hydrogen bond (see Fig. 1). Instead, the AEA amide –NH group has a hydrogen bond with water over 68.83% of the trajectory and with the DOPC ester group, 8.67%. The hydroxyl group acts as a hydrogen bond donor to water, the DOPC phosphate and the DOPC ester for 80.17%, 13.50% and 2.83%, respectively. The hydroxyl group acts as a hydrogen bond acceptor to water over 80.50% of the trajectory. Intramolecular hydrogen bonding was not detected in the AEA/TMH6 runs.

Analog results

Table 3 also presents an analysis of Analog hydrogen bonding in Runs 1 and 2. In no run of the Analog/TMH6 (Runs 1–8) did the analog headgroup form a hydrogen bond with TMH6. In Run 1 of the Analog/TMH6, the amide –NH group has a hydrogen bond with the DOPC ester group over 83.00% of the trajectory. The hydroxyl group acts as a hydrogen bond donor to water, the DOPC phosphate and the DOPC ester for 88.50%, 8.00% and 1.00% of the trajectory, respectively. The hydroxyl group acts as a hydrogen bond acceptor only to water over 86.00% of the trajectory. In Run 2 of the Analog/TMH6, the amide –NH group has a hydrogen bond with the DOPC ester group over 89.50% of the trajectory. The hydroxyl group acts as a hydrogen bond donor to water, the DOPC phosphate and the DOPC ester for 7.00%, 90.50% and 1.50%, respectively. The hydroxyl group acts as a hydrogen bond acceptor only to water over 96.50% of the trajectory. The shift in the group to which the –OH group donates a hydrogen bond is due to the higher position of the Analog headgroup in Run 2 (see below). Intramolecular hydrogen bonding was not detected in the Analog/TMH6 runs.

Bilayer group distributions

DOPC

The DOPC bilayer patch used for the runs reported here is the same as that profiled in our previous paper [30]. The group distribution for water (black) and the various DOPC moieties, phosphate (dark green), choline (red), glycerol (pink), terminal methyl (cyan) and hydrophobic core (light green) are illustrated in Fig. 2a. It is clear here that water penetrates into the

polar head group region of the DOPC bilayer. This extent of water penetration has been noted for other lipid bilayers, such as 1-stearoyl-2-docosahexaenoyl-sn-glycero-3-phosphocholine (SDPC, 18:0/22:6 PC) [35]. Chiu and co-workers found that the relatively horizontal orientation of the unsaturated bond in DOPC increases the area per lipid resulting in increased water penetration between the headgroups [36].

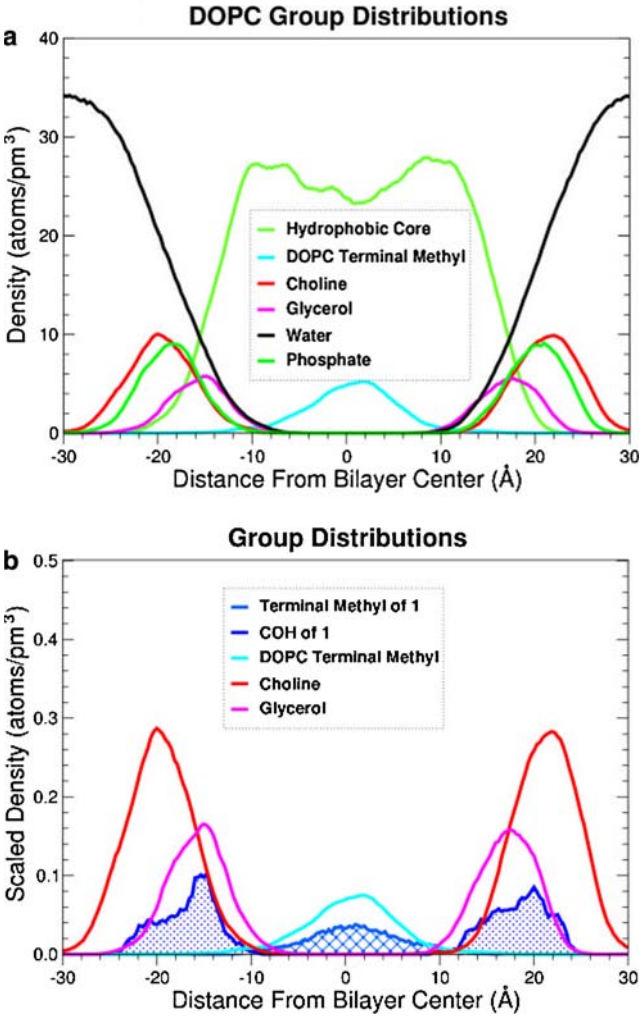

Fig. 2 (**a**) Group distributions for water (black) and the various DOPC moieties, phosphate (dark green), choline (red), glycerol (pink), terminal methyl (cyan) and hydrophobic core (light green) are illustrated here. It is clear here that water penetrates into the polar head group region of the DOPC bilayer. (**b**) Scaled group distributions of the headgroup –CH_2OH and terminal methyl of **1** with various DOPC moieties (choline, glycerol and terminal methyl) are illustrated here. Densities are scaled to the number of molecules. Here it is clear that the headgroup –CH_2OH (blue scored area) of **1** overlaps the glycerol (pink) and choline (red) moieties of the DOPC phospholipid bilayer, being centered on the glycerol group. These results indicate that on average, the headgroup hydroxyl of **1** resides in the DOPC headgroup region of the bilayer. This figure also shows the group distributions for the hydrocarbon tail (terminal methyl) of **1** (shown in blue hatched area) and the terminal methyl of DOPC (shown in cyan). It is clear here that the terminal methyl of **1** is embedded in the DOPC hydrocarbon core chain region of the bilayer with maximum density at the bilayer center [30]

AEA/DOPC

Figure 2b illustrates the scaled group distributions from our previous study of AEA in a DOPC bilayer. Here it is clear that the headgroup –CH_2OH of AEA (**1**) overlaps the glycerol and choline moieties of the DOPC phospholipid bilayer, being centered on the glycerol group. Moreover, the terminal methyl group of DOPC (cyan in Fig. 2b) lies in the center of the bilayer and does not significantly overlap the –CH_2OH group of **1** (blue scored area). These results indicate that on average, the hydroxyl headgroup of **1** resides in the DOPC headgroup region of the bilayer. Because water penetrates this DOPC headgroup region (Fig. 2a), it also can be said that the headgroup of **1** is located at the lipid/water interface. Figure 2b also shows the scaled group distributions for the hydrocarbon tail (terminal methyl) of **1** (shown in blue hatched region) and the terminal methyl region for DOPC (shown in cyan). Comparison with Fig. 2a reveals that these terminal methyls exist in the hydrocarbon core region of DOPC (shown in light green in Fig. 2a). It is clear here, then, that the terminal methyl of **1** is embedded in the DOPC hydrocarbon core chain region of the bilayer with maximum density at the bilayer center.

Group distributions for AEA in DOPC bilayer in the presence of TMH6

Figure 3a illustrates the group distributions (unscaled) for AEA in the presence of TMH6 for Run 4. Only the unscaled choline group distribution is plotted here as a reference. This distribution has been plotted over the first ns of the trajectory (1 ns; pre-P6.50 carbonyl oxygen/AEA amide –NH hydrogen bond formation), over the third ns of the trajectory (3 ns; during P6.50 carbonyl oxygen/AEA amide –NH hydrogen bond) and over the last ns of the trajectory (6 ns; post-P6.50 carbonyl oxygen/AEA amide –NH hydrogen bond). It is clear here that the headgroup –CH_2OH (solid line) resides at different positions in the bilayer over the trajectory. In the first ns slice of the trajectory, the –CH_2OH group (dark blue) distribution overlaps the choline group. In the third ns slice of the trajectory, the –CH_2OH group (red) distribution is shifted deeper in the membrane, overlapping only a fraction of the choline group region. During the last ns of the trajectory,

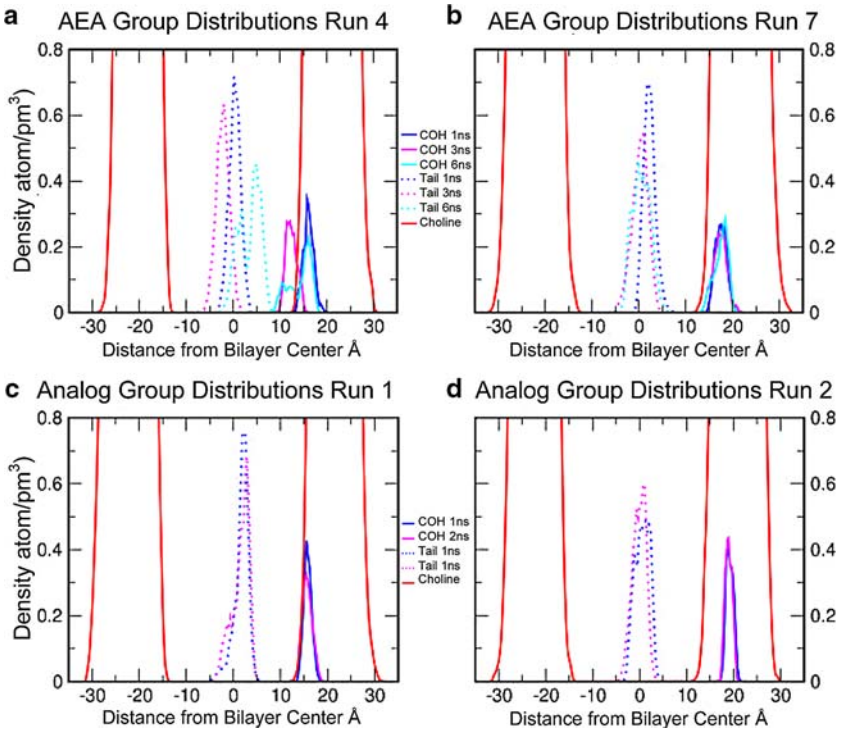

Fig. 3 Illustrated here are unscaled group distributions for (**a**) AEA Run 4 and (**b**) AEA Run 7 over the first (dark blue), third (red) and final (cyan) ns of the trajectory; and, for (**c**) Analog Run 1 (**d**) Analog Run 2 over the first (dark blue) and second (red) ns of the trajectory. The unscaled distribution for the choline group in DOPC is shown in orange as a reference. The position of the headgroup –CH_2OH is shown in solid lines, while the position of the terminal methyl is shown in dashed lines

the –CH_2OH group (cyan) distribution is bimodal, with the –CH_2OH group in early parts of the trajectory below the choline region, while in later parts of the trajectory, the –CH_2OH group distribution overlaps with the choline distribution. Figure 4 illustrates the position of AEA in the bilayer at 1 ns, 3 ns and 6 ns (Run 4). This figure shows that when AEA is engaged in the amide –NH/ P6.50 backbone carbonyl oxygen hydrogen bond (3 ns, Fig. 4b), the headgroup of the ligand lies lower in the bilayer compared with its position earlier in the simulation at 1 ns or at the end of the simulation (6 ns). The V6.43/I6.46 groove lies near the middle of the DOPC bilayer. The distributions for the terminal methyl of AEA (dotted lines in Fig. 3a) show that the terminal methyl tail lies on average at the center of the bilayer during the first ns slice (dark blue dotted line). The tail lies on average deeper in the membrane during the third ns slice (pink dotted line). This deeper position reflects the fact that more of the pentyl/alkyl tail carbons are inserted in the V6.43/I6.46 groove (compare alkyl chain position in Fig. 4a with b). The last ns of the trajectory shows a bimodal distribution, with the tail being located near the membrane center early in the trajectory and then sitting higher in the bilayer during the latter part of this time slice (cyan dotted line). Figure 4c (right) illustrates the position of AEA in the membrane at the end of the trajectory. It is clear here that AEA has assumed a more U shaped conformation, causing the tail to sit higher in the bilayer. This produces the shallower position for the terminal methyl in the bilayer seen in the group distributions for the last ns of the trajectory (Fig. 3a, cyan dotted line).

Figure 3b illustrates the group distributions for the AEA –CH_2OH and pentyl/alkyl tail terminal methyl in the bilayer at 1 ns (dark blue), 3 ns (red) and 6 ns (cyan) for Run 7. The group distributions for Run 7 show less variation in the location of AEA in the bilayer during the first, third and last ns of the trajectory. The distributions for the –CH_2OH group overlap with the choline distribution at each time frame, while the terminal tail methyl lies on average near the center of the bilayer.

Group distributions for analog in DOPC bilayer in the presence of TMH6

Frequent interactions of the Analog acyl/alkyl chain with the V6.43/I6.46 groove were seen early in the trajectories (typically first 2 ns, see Table 1). Figure 3c illustrates the group distributions (unscaled) for the Analog in the presence of TMH6 for Run 1. The distributions for the –CH_2OH group (1 ns, dark blue solid line; 2 ns pink solid line), overlap with the choline distribution at 1 ns and at 2 ns, while the terminal tail methyl (1 ns dark blue dotted line; 2 ns pink dotted line) lies on average near the center of the bilayer, slightly shifted extracellular (i.e., to the right in Fig. 3c). Figure 3d illustrates the Run 2 group distributions (unscaled) for the –CH_2OH group and acyl/

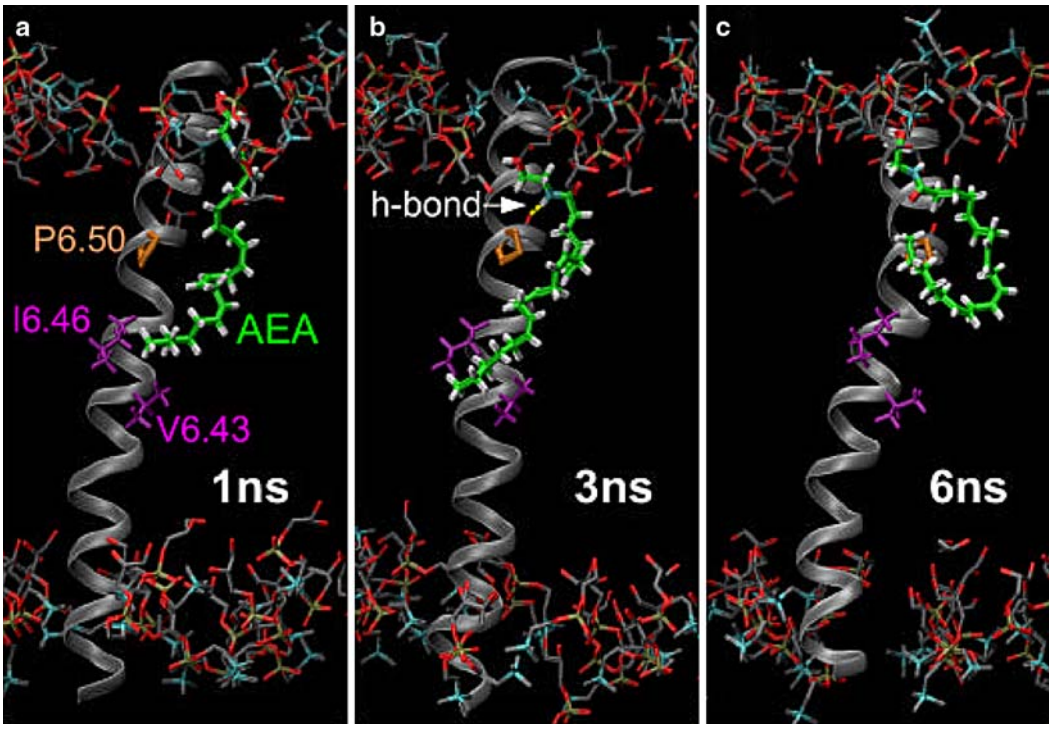

Fig. 4 The position of AEA in the DOPC bilayer at (**a**) 1 ns, (**b**) 3 ns and (**c**) 6 ns relative to TMH6 and the V6.43/I6.46 groove for Run 4 is illustrated here. The choline (blue) and phosphate (gold) groups of the DOPC bilayer are shown in tube display. The acyl chains of the bilayer, as well as the waters have been eliminated to simplify the display. The helix backbone of TMH6 is shown in ribbon display, colored gray. AEA is shown in tube display with carbon atoms colored green. The V6.43/I6.46 groove (colored purple), as well as P6.50 (colored orange) are shown in tube display. This figure shows that when AEA is engaged in a hydrogen bond between the amide –NH and P6.50 backbone carbonyl oxygen (3 ns, **b**), the headgroup of the ligand lies lower in the bilayer compared with its positions earlier in the simulation at 1 ns (**a**) or at the end of the simulation (6 ns, **c**). The acyl chain is inserted into the V6.43/I6.46 groove at 3 ns (**b**), while at 6 ns (**c**), the acyl tail is higher in the membrane

alkyl chain terminal methyl group of the Analog in the bilayer during the first and second ns of the trajectory. The distributions for the $-CH_2OH$ group (1 ns, dark blue solid line; 2 ns pink solid line) overlap with the choline distribution, but they are less deep in the bilayer while the terminal tail methyl (1 ns dark blue dotted line; 2 ns pink dotted line) lies on average near the center of the bilayer. Figure 5 illustrates the position of the analog in the bilayer at the end of the second ns of Run 2. Here it is clear that the Analog is in an extended conformation that allows the $-CH_2OH$ group to be much higher in the bilayer, while the terminal tail methyl is still located near the bilayer center at the level of the V6.43/I6.46 groove.

Discussion

Our previous MD simulations have shown that in the absence of TMH6, AEA forms short-lived (~0.10–0.25 ns) hydrogen bonds with lipid bilayer constituents and with water that has penetrated into the lipid bilayer [30]. In the simulations reported here, both AEA or Analog and TMH6 were incorporated into the DOPC bilayer. These simulations show a higher tendency for AEA to associate with the TMH6 V6.43/I6.46 groove than does the Analog (Table 1). Our simulations also show that AEA or the Analog (in the outer leaflet of the bilayer) competes with lipids for interaction with the V6.43/I6.46 groove. In most cases these lipids are from the sn–1 chain and are from the inner leaflet of the bilayer. The average energy of interaction between the Analog and TMH6 in a trajectory with little groove interaction (Analog Run 1(2 ns)) is comparable to the energy of interaction between AEA and TMH6 in a trajectory where there is little groove interaction (AEA Run 7(6 ns)) (see Table 2). In trajectories where groove interaction was more frequent (AEA Run 4 and Analog Run 2), average energies of interaction were larger, although only the energy of interaction of AEA/TMH6 in Run 4 was found to be statistically different from the other runs in Table 2. In this case, hydrogen bonding distance was maintained between the AEA amide –NH group and the P6.50 backbone carbonyl oxygen over ~3.5 ns of the trajectory (see Fig. 1). A re-run of Run 4

(see Methods) resulted in this hydrogen bond distance lasting ~5 ns (data not shown here). There are three elements of the endocannabinoid system that appear to be important to facilitate this higher interaction energy between AEA and TMH6 in Run 4: (1) the TMH6 $\beta XX\beta$ groove motif, (2) acyl chain flexibility and (3) the kink induced by the CWXP motif in CB1 TMH6. Each of these elements is discussed below:

Importance of groove

Our modeling studies have suggested that β branched amino acids Val, Ile or Thr located (i, i + 3) or (i, i + 4) apart on an alpha helix can form a groove into which a ligand alkyl chain can fit [19]. The MD simulations reported here are consistent with this result, as these showed that the pentyl/alkyl tail of AEA, the Analog and even the last five carbons of the DOPC (sn–1 chain usually) from the lower leaflet can interact with the V6.43/I6.46 groove which is situated at the center of the bilayer (see Fig. 4, purple residues and Table 1).

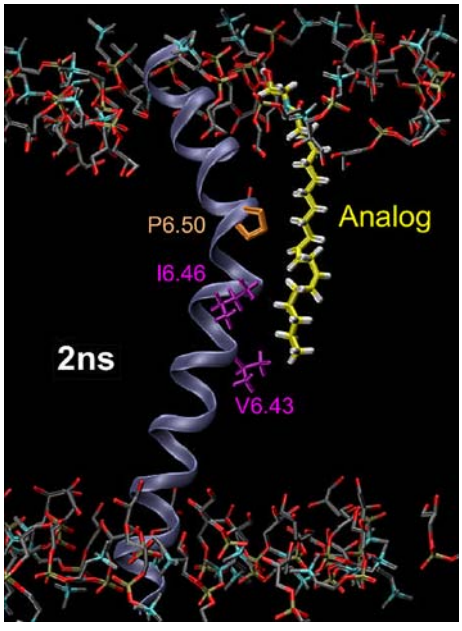

Fig. 5 The position of the (20:2, *n*–6) analog in the DOPC bilayer at 2 ns relative to TMH6 and the V6.43/I6.46 groove for Run 2 is illustrated here. The choline (blue) and phosphate (gold) groups of the DOPC bilayer are shown in tube display. The acyl chains of the bilayer, as well as the waters have been eliminated to simplify the display. The helix backbone of TMH6 is shown in ribbon display, colored gray. The Analog is shown in tube display, with carbon atoms colored yellow. The V6.43/I6.46 groove (colored purple), as well as P6.50 (colored orange) are shown in tube display. Here it is clear that the Analog is in an extended conformation that allows the $-CH_2OH$ group to rise higher in the bilayer, while the terminal tail methyl is still located near the bilayer center. At this timepoint (2 ns), there is no groove interaction

Experimental support for a $\beta XX\beta$ motif being a more general motif for alkyl chain recognition/interaction comes from the crystal structure of adipocyte lipid binding protein (ALBP) complexed with stearic acid [37] in which the fatty acid tail is threaded through a groove formed by T29 and V32 on the α-II portal helix [38]. Interestingly, support also comes from the crystal structure of FAAH, the enzyme that degrades AEA, complexed with the inhibitor adduct methoxy arachidonyl phosphonate, MAP) [5]. Several beta branching amino acids (T488, I491 and V495) are located on a helical segment in the channel leading to the active site. These appear to help thread the arachidonyl chain into the helical/S shaped acyl-chain binding channel. Mutation studies of one of these residues, Ile491 have shown that this residue participates in substrate recognition [39]. Thus, the endocannabinoid system may use beta branchers to facilitate ligand recognition/interaction for more protein targets than just the CB1 receptor.

The TMH6 $\beta XX\beta$ motif at residues 6.43/6.46 is found in a limited set of other GPCRs. In 2003, Mirzadegan and co-workers published a survey of the amino acid composition of 270 Class A GPCRs. This survey indicated that the occurrence of beta branching residues (V, I or T) at position 6.43 in TMH6 was 34%, 9% and 11%, respectively; while at position 6.46, this occurrence was 28%, 21% and 1%, respectively (see Supporting Information, Helix-VI) [40]. These results show that it is not uncommon for a beta branching residue to occur at position 6.43 or at position 6.46. This is consistent with the hydrophobic nature of these amino acids and the lipid bilayer environment of these lipid facing residues. (Threonines can exist in a hydrophobic environment by forming intrahelical hydrogen bonds between the O-γ atom and the i–3 or i–4 carbonyl oxygen [41]). Mirzadegan and co-workers' statistics do not indicate, however, how frequently beta branchers simultaneously occupy both position 6.43 and 6.46, for only then would a groove be formed.

Our survey of human data from the current GPCR sequence data base for Class A GPCRs (1141 receptors) (see http://www.gpcr.org/7 tm/seq/DRlist.html#001) revealed that this motif is found in only 57 GPCRs including CB1. This set of 57 receptors includes other receptors with lipid-derived ligands such as the cannabinoid CB2 receptor and two putative cannabinoid receptors (GPR35 and GPR55), lysosphingolipid/lysophosphatidic acid/S1P-type receptors (GPR4, GPR34, GPR63, EDG-5), prostanoid receptors (TA2R, PF2R, PE2R3, PE2R2), and an oxoeico-

sanoid receptor (OXER1). This group clearly represents only a sub-set of GPCRs with lipid-derived ligands. However, we have shown here that a groove at 6.43/6.46 is located at the proper depth to interact with arachidonic acid derivatives and not with fatty acid derivatives of other lengths or unsaturation patterns. Presumably, interaction with fatty acid chains of differing lengths/unsaturation patterns would require groove location at different depths in the bilayer. Inspection of TMH6 sequences of the Lysosphingolipid and LPA (EDG) Class A GPCRs (http://www.gpcr.org/7 tm/seq/001_014/001_014.html) and Prostanoid Class A GPCRs (http://www.gpcr.org/7 tm/seq/001_006/001_006.html) reveals that all have a groove(s) present on TMH6 at various positions intracellular to the CWXP motif.

The group of 57 Class A GPCRs that possess β branchers at 6.43/6.46 also includes peptide, amine, nucleotide, nicotinic and orphan receptors. The existence of the groove at this level on TMH6 in these receptors may represent a ligand interaction site or a lipid modulation site. *Most importantly, only two Class A GPCRs have both beta branchers at 6.43/6.46 and a Gly at 6.49.* These are CB1 and the protease-activated Thrombin Receptor (PAR1; I6.43, I6.46, G6.49) [42]. Thus, the occurrence of this combined motif is quite rare, 0.18% across Class A GPCRs. PAR1 is the principal thrombin receptor in humans, mediating thrombin induced aggregation of platelets and adverse events, such as proinflammatory responses, angiogenesis, cell invasion, and neurodegeneration in other cell types [43]. Human vascular endothelial cells have been reported to generate and release the endocannabinoid, 2-arachidonoylglycerol upon stimulation with thrombin [44]. Recently, extracts of cannabis and the classical cannabinoids (Δ^9-THC, CBD and CBN) have been shown to have antithrombic effects [45]. It is tempting to speculate, therefore that the combination of the I6.43/I6.46 groove and G6.49 in PAR1 may permit recognition of classical and endocannabinoids that leads to antagonism of thrombin effects.

We show here (Table 1) that the CB1 endogenous ligand, AEA (**1**) exhibits a higher incidence of V6.43/I6.46 groove interaction, which in some cases leads to a sustained interaction with TMH6. On the other hand, the (20:2, *n*–6) Analog (**6**) which has essentially no affinity for CB1, shows a lower incidence of V6.43/I6.46 groove interaction (see Table 1) and does not appear to be able to engage in a sustained interaction with TMH6. These results support the hypothesis that the TMH6 V6.43/I6.46 groove may selectively interact with AEA over its (20:2, *n*–6) analog in lipid, *however, this groove interaction alone appears to be a necessary, but not a sufficient condition to ''fish'' AEA out of lipid.*

Acyl chain flexibility in TMH6 interaction

Another key feature of the endocannabinoid system that appears to contribute to AEAs ability to interact with TMH6 is the flexibility of its arachidonic acid unsaturated acyl chain. One important feature of this chain is the great torsional mobility about the Csp^2–Csp^3 bonds. The energy barrier for rotation about the Csp^2–Csp^3 bonds present in the homoallylic double bond region of molecules like arachidonic acid is 1.3 kcal/mol [28]. In contrast, the torsional barrier for rotation about Csp^3–Csp^3 bonds in straight chain alkanes is approximately 3 kcal/mol [46]. This difference in rotational energy barriers results in high equilibrium flexibility for polyunsaturated acyl chains compared with saturated acyl chains [47, 48]. *The consequence of the presence of homoallylic double bonds in an acyl chain is the ability to adopt many conformations from extended to curved shapes.* This is clearly seen in our previous Monte Carlo/simulated annealing conformational analysis study of AEA versus the (20:2, n–6) analog in a continuum solvation model of chloroform [49]. For AEA (20:4, *n*–6), 49 out of 100 conformers were in a U shape (Cls 1) in which the four homoallylic double bonds formed the curved portion of the U, bringing the head and tail close together. Twenty-nine out of 100 conformers of AEA (Cls 2) were in an extended conformation. For the (20:2, *n*–6) analog, 19 conformers out of 100 conformers formed a broad U-shaped cluster (Cls 1), with the curvature occurring in the region of the two homoallylic double bonds; while 41 out of 100 conformers were in extended conformations (Cls 2). The (20:2, *n*–6) analog U-shaped family (Cls 1) had an average radius of curvature of 5.8 Å (5.3–6.2) which was statistically different from the 4.0 Å (3.7–4.2) radius of curvature of AEA Cls 1 [49].

This difference in flexibility between AEA and the Analog is also seen here in our simulations with TMH6 in DOPC. In the presence of TMH6, AEA (in Run 4) can form a long lasting interaction with TMH6 by first associating with the V6.43/I6.46 groove and then molding itself to the lipid face of TMH6 (Fig. 4b). This ability to ''mold'' its shape most likely stems from the homoallylic double bond structure of arachidonyl acyl chain in AEA which gives the molecule tremendous flexibility in this homoallylic double bond region of the acyl chain, allowing it to curve around P6.50 to reach the exposed backbone carbonyl oxygen. The resultant conformation of AEA bears a striking resemblance to

Cluster 1 for the isolated AEA in our previous paper (see Fig. 1 in [49]). While the Analog does have two double bonds separated by a methylene carbon near the end of its acyl chain, it lacks such structure nearer the headgroup and therefore is not capable of ''molding'' the region nearer the headgroup to the lipid face of TMH6 to achieve a hydrogen bond. Instead, the Analog's profile in the membrane relative to TMH6 looks more typically like that shown in Fig. 5, which bears a striking resemblance to the extended cluster (Cluster 2) for the isolated Analog in our previous paper (see Fig. 1 in [49]).

As evidenced in Table 2, a high average energy of interaction is achieved only when AEA can establish a hydrogen bonding interaction with TMH6, while maintaining its groove interaction. The resultant compounded interaction has both greater electrostatic and Van der Waals components to the energy, resulting in an additional 9.60 kcal/mol of interaction energy, for example, over AEA Run 7. We saw this compounded interaction between TMH6 and AEA in one out of eight initial trajectories and were able to reproduce this interaction in a re-run. Under physiological conditions, it is likely that there will be many AEA molecules in the vicinity of TMH6. This higher concentration of AEA should result in a more frequent occupation of the groove by AEA, increasing the likelihood of the ''compounded'' interaction.

TMH6 CWXP motif

The third feature of the endocannabinoid system that appears to contribute to AEAs ability to interact with TMH6, is the availability of the P6.50 backbone carbonyl oxygen. We have seen in Run 4 that the availability of the P6.50 backbone carbonyl facilitates the hydrogen bonding interaction of AEA with TMH6 pictured in Fig. 4b. The availability of this backbone carbonyl arises from the specific sequence of the CWXP flexible hinge motif present in CB1 TMH6, CWGP. Due to the technical difficulties associated with crystallizing transmembrane proteins such as the GPCRs [50], only one GPCR, the Class A receptor, rhodopsin (Rho) has been crystallized to date [51–53]. This structure, which represents the Rho dark-adapted (inactive state), has become the ''gold standard'' for homology modeling of other Class A GPCRs. While current research efforts are directed towards obtaining a structure of the Rho activated state (Meta II) [54, 55], at present our primary structural information about the GPCR activation process comes from biophysical studies of Rho, the beta-2-adrenergic receptor (β2-AR) and the M_3 muscarinic receptor. These studies have indicated that rotation of both TMHs 3 and 6, as well as a conformational change in TMH6 (straightening in the CWXP hinge region of TMH6) occurs upon GPCR activation [56–62]. Both CB1 (CWGP) and CB2 (CWFP) possess the TMH6 CWXP hinge motif common to Class A GPCRs. Our Monte Carlo/simulated annealing (Conformational Memories) study of TMH6 in CB1 versus CB2 revealed a significant difference in the flexibility of the CWXP region, however, between these two helices (see Fig. 5 in [19]). For CB1, the average kink angle was 40.9° (std. deviation ± 16.9°); while for CB2, the average kink angle was 24.6° (std. deviation of ± 4.3°). In silico CB1 G6.49F and CB2 F6.49G swap mutant studies revealed that the profound flexibility of WT CB1 TMH6 is largely due to the presence of the small residue (Gly) at position 6.49, the X of CWXP [19]. The TMH6 conformer used here in our DOPC simulations was taken from this Conformational Memories study of CB1 TMH6 and is the same helix conformer that we have incorporated into our model of the CB1 inactive state [63]. *One important result of the profound flexibility in CB1 TMH6 is that the P6.50 backbone carbonyl is very exposed*.

Implications of AEA/TMH6 interaction for CB1 signaling

The purpose of the MD studies presented here was to assess if AEA was located in the bilayer at the proper depth and orientation to engage in an interaction with the lipid face of TMH6 and if this interaction involved the V6.43/I6.46 groove. In calculations that are currently underway, we are testing whether AEA can interact with the lipid face of TMH6 in the context of the full CB1 TMH bundle embedded in lipid via multinanosecond MD studies. Initial results indicate that the TMH6 groove residues are accessible to AEA in the context of the full CB1 bundle. The fact that the V6.43A/I6.46A double mutation in CB1 separates the binding sites of ligands from structural classes with required alkyl/acyl tails (classical, non-classical and endogenous cannabinoids) from those that lack such functionality (aminoalkylindoles and biarylpyrazoles) [20] provides experimental support for the importance of the V6.43/I6.46 groove in CB1 ligand binding.

We have shown previously that alkyl chain interaction with the V6.43/I6.46 groove in CB1 TMH6 (in $CHCl_3$) can lead to a straightening in the CWXP flexible hinge region [19]. This straightening has been associated with activation of GPCRs [56, 57, 60]. In some of the MD runs reported here, we did observe TMH6 straightening during AEA interaction. How-

ever, it is not possible to conclude at this point that the initial AEA interaction with CB1 TMH6 in the lipid bilayer produces receptor activation, since only TMH6 was present in the current simulations. We have envisioned that if straightening of TMH6 does occur, and is accompanied by a counterclockwise rotation, AEA (hydrogen bonded to TMH6) could possibly be introduced into the CB1 TMH binding pocket. Such access to the interior of the TMH binding pocket may be facilitated by the helix discontinuity in TMH7 at the level of P6.50 [51] which may allow easy passage of the bulkier headgroup region of AEA into the TMH bundle interior. However, modeling the entire process will likely require the use of steered MD, calculations that are also planned for the future.

Implications for endocannabinoid SAR

The work reported here is a continuation of work [19, 49, 64] we initiated to explore the molecular origins for the very restrictive endocannabinoid acyl chain SAR which dictates that only 20–22 carbon, *n*–6 endocannabinoids with 3 or more homoallylic double bonds display high affinity for CB1 [13]. We have shown here that the ability to form a strong interaction with the lipid face of TMH6 for 20 carbon, *n*–6 endocannabinoids depends upon acyl chain flexibility induced by the presence of 4 versus 2 homoallylic double bonds. While we have not reported here runs in which the number of carbons in the acyl chain was varied, inspection of Fig. 4b would suggest that an acyl chain shorter than 20 carbons may not permit the endocannabinoid to arch around P6.50 to establish the hydrogen bond and an acyl chain longer than 22 carbons (which will increase the run of saturated carbons near the head group), may then lack the flexibility to correctly place the NH group for hydrogen bond interaction. Work is currently underway in our laboratory to test these hypotheses as well.

Conclusions

We have shown here that the acyl/alkyl tail of the CB1 endogenous ligand, AEA is located at the correct depth in the bilayer to interact with the $\beta XX\beta$ motif, V6.43/I6.46 groove on the lipid face of CB1 TMH6 and that AEA has a higher propensity for interacting with this groove than the low CB1 affinity (20:2, *n*–6) analog of AEA. AEA can have a high energy of interaction with TMH6 by first associating with the V6.43/I6.46 groove and then molding itself to the lipid face of TMH6 to establish a hydrogen bonding interaction with the exposed backbone carbonyl of P6.50. AEAs ability to ''mold'' itself to the lipid face of TMH6 most likely stems from the homoallylic double bond structure of its arachidonyl acyl chain which gives the molecule tremendous flexibility in this allylic double bond region of the acyl chain. While the (20:2, *n*–6) analog of AEA does have a set of homoallylic double bonds near the end of its acyl chain, it lacks such functionality nearer the headgroup and therefore is not capable of ''molding'' the region nearer the headgroup to the lipid face of TMH6 to establish the analogous hydrogen bonding interaction.

Acknowledgements This work was supported by NIDA grants DA03934 and DA000489 (PHR) and supercomputing support was provided by the Pittsburgh Supercomputer Center, AAB grant numbers MCB030006P and MCB030017. This work was also supported by the Theoretical and Computational Biophysics group, an NIH Resource for Macromolecular Modeling and Bioinformatics, at the Beckman Institute, University of Illinois at Urbana–Champaign, through the use of the software packages NAMD2 and VMD (Figs. 4 and 5 were prepared using VMD). The authors wish to thank Dow Hurst and Judy Barnett-Norris for their technical assistance in the preparation of this manuscript.

References

1. Di Marzo V, Melck D, Bisogno T, De Petrocellis L (1998) Trends Neurosci 21:521
2. Piomelli D, Beltramo M, Giuffrida A, Stella N (1998) Neurobiol Dis 5:462
3. Devane WA, Hanus L, Breuer A, Pertwee RG, Stevenson LA, Griffin G, Gibson D, Mandelbaum A, Etinger A, Mechoulam R (1992) Science 258:1946
4. McFarland MJ, Porter AC, Rakhshan FR, Rawat DS, Gibbs RA, Barker EL (2004) J Biol Chem 279:41991
5. Bracey MH, Hanson MA, Masuda KR, Stevens RC, Cravatt BF (2002) Science 298:1793
6. Gerard CM, Mollereau C, Vassart G, Parmentier M (1991) Biochem J 279(Pt 1):129
7. Mechoulam R, Ben-Shabat S, Hanus L, Ligumsky M, Kaminski NE, Schatz AR, Gopher A, Almog S, Martin BR, Compton DR et al (1995) Biochem Pharmacol 50:83
8. Hanus L, Abu-Lafi S, Fride E, Breuer A, Vogel Z, Shalev DE, Kustanovich I, Mechoulam R (2001) Proc Natl Acad Sci USA 98:3662
9. Porter AC, Sauer JM, Knierman MD, Becker GW, Berna MJ, Bao J, Nomikos GG, Carter P, Bymaster FP, Leese AB, Felder CC (2002) J Pharmacol Exp Ther 301:1020
10. Reggio PH (2005) Handb Exp Pharmacol 247
11. Thakur GA, Duclos RI Jr, Makriyannis A (2005) Life Sci 78:454
12. Mahadevan A, Razdan RK (2005) Aaps J 7:E496
13. Sheskin T, Hanus L, Slager J, Vogel Z, Mechoulam R (1997) J Med Chem 40:659
14. Reggio PH, Traore H (2000) Chem Phys Lipids 108:15
15. Palmer SL, Khanolkar AD, Makriyannis A (2000) Curr Pharm Des 6:1381
16. Pinto JC, Potie F, Rice KC, Boring D, Johnson MR, Evans DM, Wilken GH, Cantrell CH, Howlett AC (1994) Mol Pharmacol 46:516

17. Berglund BA, Boring DL, Howlett AC (1999) Adv Exp Med Biol 469:527
18. Berglund BA, Fleming PR, Rice KC, Shim JY, Welsh WJ, Howlett AC (2000) Drug Des Discov 16:281
19. Barnett-Norris J, Hurst DP, Buehner K, Ballesteros JA, Guarnieri F, Reggio PH (2002) Int J Quantum Chem 88:76
20. Reggio PH, Nebane NM, Lynch DL, Song Z-H (2005) In: Musty R (ed) 2005 Symposium on the Cannabinoids, vol 15. ICRS, Clearwater, Florida, p 21
21. Sawzdargo M, Nguyen T, Lee DK, Lynch KR, Cheng R, Heng HH, George SR, O'Dowd BF (1999) Brain Res Mol Brain Res 64:193
22. Drmota T, Greasley P, Groblewski T (2004). Astrazeneca, USA
23. O'Dowd BF, Nguyen T, Marchese A, Cheng R, Lynch KR, Heng HH, Kolakowski LF Jr, George SR (1998) Genomics 47:310
24. Kale L, Skeel R, Bhandaarkar M, Brunner R, Gursoy A, Krawetz N, Phillips J, Shinozaki A, Varadarajan K, Schulten K (1999) J Comp Phys 151:283
25. Schlenkrich M, Brickmann J, MacKerell AD, Jr., Karplus M (1996) In: Merz KM, Roux B (eds) Biological membranes: a molecular perspective from computation and experiment. Birkhauser, Boston, MA, p 31
26. MacKerell AD Jr, Bashford D, Bellot M, Dunbrack RL Jr, Evanseck J, Field MJ, Fischer S, Gao J, Guo H, Ha S, Joseph D, Kuchnir L, Kuczera K, Lau FT K, Mattos C, Michnick S, Ngo T, Nguyen DT, Prodhom B, Reiher IWE, Roux B, Schlenkrich M, Smith J, Stote R, Straub J, Watanabe M, Wiorkiewicz-Kuczera J, Yin D, Karplus M (1998) J Phys Chem B 102:3586
27. Feller SE, MacKerell AD Jr (2000) J Phys Chem B 104:7510
28. Feller SE, Gawrisch K, MacKerell AD Jr (2002) J Am Chem Soc 124:318
29. Darden TA, York D, Pedersen L (1993) J Chem Phys 98:10089
30. Lynch DL, Reggio PH (2005) J Med Chem 48:4824
31. Bhandarkar M, Brunner R, Chipot C, Dalke A, Dixit A, Grayson P, Gullingsrud J, Gursoy A, Hardy D, Humphrey W, Hurwitz D, Krawetz N, Nelson M, Phillips J, Shinozaki A, Zheng G, Zhu F (2006) NAMD2 User's Guide, Version 2.6, http://www.ks.uiuc.edu/Research/namd/2.6/ug
32. Humphrey W, Dalke A, Schulten K (1996) J Mol Graph 14:33
33. Elmore DE, Dougherty DA (2003) Biophys J 85:1512
34. Ballesteros JA, Weinstein H (1995) In: Sealfon SC (ed) Methods in neuroscience, vol 25. Academic Press, San Diego, CA, p 366
35. Saiz L, Klein ML (2001) Biophys J 81:204
36. Chiu SW, Jakobsson E, Subramaniam S, Scott HL (1999) Biophys J 77:2462
37. Xu Z, Bernlohr DA, Banaszak LJ (1992) Biochemistry 31:3484
38. Xu Z, Bernlohr DA, Banaszak LJ (1993) J Biol Chem 268:7874
39. Patricelli MP, Cravatt BF (2001) Biochemistry 40:6107
40. Mirzadegan T, Benko G, Filipek S, Palczewski K (2003) Biochemistry 42:2759
41. Ballesteros JA, Deupi X, Olivella M, Haaksma EE, Pardo L (2000) Biophys J 79:2754
42. Skorkowska K, Adamiec R (2005) Int Angiol 24:215
43. Day JR, Punjabi PP, Randi AM, Haskard DO, Landis RC, Taylor KM (2004) Circulation 110:2597
44. Sugiura T, Kodaka T, Nakane S, Kishimoto S, Kondo S, Waku K (1998) Biochem Biophys Res Commun 243:838
45. Coetzee C, Levendal RA, van de Venter M, Frost CL (2006) Phytomedicine, April 25, Epub
46. Smith GD, Jaffe RL (1996) J Phys Chem 100:18718
47. Rabinovich AL, Ripatti PO (1991) Biochim Biophys Acta 1085:53
48. Rich MR (1993) Biochim Biophys Acta 1178:87
49. Barnett-Norris J, Hurst DP, Lynch DL, Guarnieri F, Makriyannis A, Reggio PH (2002) J Med Chem 45:3649
50. Sarramegn V, Muller I, Milon A, Talmont F (2006) Cell Mol Life Sci 63:1149
51. Palczewski K, Kumasaka T, Hori T, Behnke CA, Motoshima H, Fox BA, Le Trong I, Teller DC, Okada T, Stenkamp RE, Yamamoto M, Miyano M (2000) Science 289:739
52. Okada T, Fujiyoshi Y, Silow M, Navarro J, Landau EM, Shichida Y (2002) Proc Natl Acad Sci USA 99:5982
53. Li J, Edwards PC, Burghammer M, Villa C, Schertler GF (2004) J Mol Biol 343:1409
54. Schertler GF (2005) Curr Opin Struct Biol 15:408
55. Szundi I, Ruprecht JJ, Epps J, Villa C, Swartz TE, Lewis JW, Schertler GF, Kliger DS (2006) Biochemistry 45:4974
56. Farrens D, Altenbach C, Ynag K, Hubbell W, Khorana H (1996) Science 274:768
57. Ghanouni P, Steenhuis JJ, Farrens DL, Kobilka BK (2001) Proc Natl Acad Sci USA 98:5997
58. Lin SW, Sakmar TP (1996) Biochemistry 35:11149
59. Javitch JA, Fu D, Liapakis G, Chen J (1997) J Biol Chem 272:18546
60. Jensen AD, Guarnieri F, Rasmussen SG, Asmar F, Ballesteros JA, Gether U (2001) J Biol Chem 276:9279
61. Nakanishi J, Takarada T, Yunoki S, Kikuchi Y, Maeda M (2006) Biochem Biophys Res Commun 343:1191
62. Ward SD, Hamdan FF, Bloodworth LM, Siddiqui NA, Li JH, Wess J (2006) Biochemistry 45:676
63. McAllister SD, Hurst DP, Barnett-Norris J, Lynch D, Reggio PH, Abood ME (2004) J Biol Chem 279:48024
64. Barnett-Norris J, Guarnieri F, Hurst DP, Reggio PH (1998) J Med Chem 41:4861